Hindawi Publishing Corporation
Journal of Nanomaterials
Volume 2011, Article ID 529874, 10 pages
doi:10.1155/2011/529874

Research Article

Hydrothermal Synthesis of SnO_2 Nanostructures with Different Morphologies and Their Optical Properties

Lin Tan, Lihong Wang, and Yude Wang

Department of Materials Science and Engineering, Yunnan University, 650091 Kunming, China

Correspondence should be addressed to Yude Wang, ydwang@ynu.edu.cn

Received 15 January 2011; Accepted 20 March 2011

Academic Editor: Hongchen Chen Gu

SnO_2 hollow spheres and nanorods were prepared by an aqueous sol-gel route involving the reaction of tin chloride and sodium dodecyl sulphate (SDS) in hexanol and heptane under the different hydrothermal treating temperature and time. X-ray diffraction (XRD) spectra, Fourier transformed infrared (FTIR) spectrum, scanning electron microscopy (SEM), transmission electron microscopy (TEM), high-resolution TEM (HRTEM) and Raman spectroscopy were used to examine the morphology and microstructure to find out the cause. The result indicates that the products are hollow spheres with diameters of approximately 200–900 nm and shell thickness of 60–70 nm via hydrothermal treating at 160°C and one-dimensional rod-like nanostructures with diameters of approximately 20–40 nm and lengths of 100–300 nm via hydrothermal treating at 180 and 200°C, respectively. Room-temperature photoluminescence (PL) properties were investigated under the excitation of 275 nm. The samples exhibited the emission peaks of room-temperature photoluminescence.

1. Introduction

Rutile tin oxide is an n-type semiconductor oxide with a wide energy gap (E_g = 3.62 eV, at 300 K). It is particularly interesting, because it has high chemical stability and excellent optical and electrical properties and has been widely used as a catalyst for oxidation of organic compounds, and as gas sensors [1, 2], rechargeable Li-batteries, and optical electronic devices [3, 4]. The physical and chemical properties of tin oxide nanocrystalline material often differ from crystalline or amorphous ones. These properties are dictated to a large extent by crystal structure and morphology as well as by grain size. The synthesis of tin oxide nanostructures with desired structure and morphology is of great technological and scientific interest owing to their superior physical and chemical properties and such a large range of applications such as, gas sensors, photocatalysts, nanofiltration membranes, heat mirrors, glass coatings, and electrochromic windows. Thus, it is very important to develop ways for controlling their dimensions, structure, surface, and interface properties.

Many methods for the fabrication of SnO_2 nanostructures have been developed, ranging from lithographic technologies to chemical methods [5, 6]. Because of its advantages, the role of chemistry in materials science has been rapidly growing. Various chemical methods are adopted for the preparation of nanometer tin oxide include the gas-phase methods [7–9], sol-gel methods [10–12], evaporative decomposition of solution [7, 13], laser ablation technique [14], and wet chemical synthesis [15–21]. The wet-chemical synthesis possesses the advantage of producing nanomaterials with uniform structure in large scale. Recently, Krishna and Komarneni [22] used both conventional-hydrothermal and microwave-hydrothermal methods to prepare SnO_2 nanoparticles of very high surface areas. The synthesis of these nanostructures is based on the preparation of tin precursor precipitates and the subsequent hydrothermal treatment at a designated temperature. Among them, the hydrothermal method is widely used to prepare the nanostructural materials because of its simplicity, high efficiency, and low cost. On the other hand, the nanostructure morphologies are tuned by changing experimental parameters. It is known that the time-temperature history of the process has a strong influence on the crystal structure and morphology of nanostructured materials [23]. In this work, we have synthesized

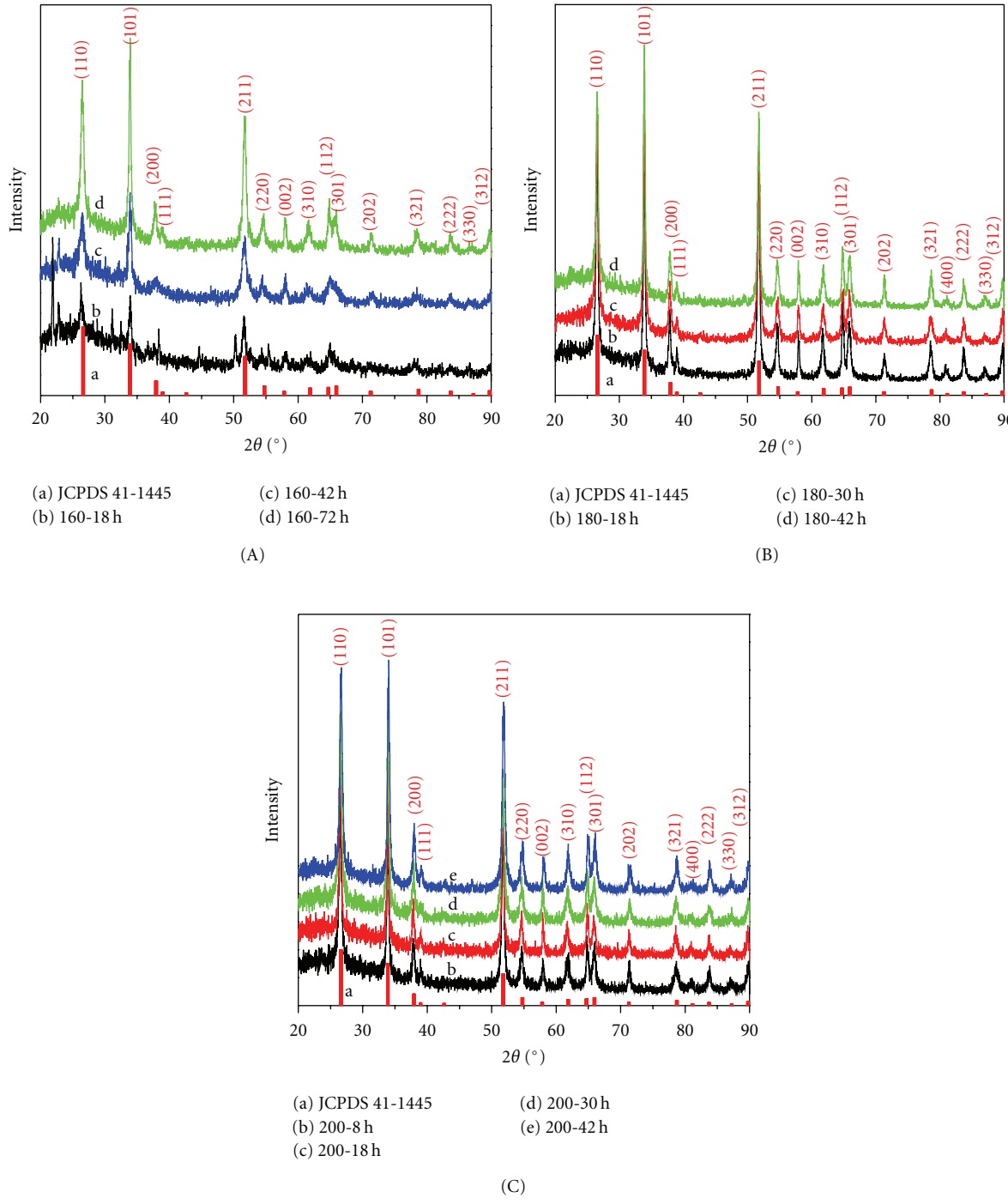

(a) JCPDS 41-1445
(b) 160-18 h
(c) 160-42 h
(d) 160-72 h

(A)

(a) JCPDS 41-1445
(b) 180-18 h
(c) 180-30 h
(d) 180-42 h

(B)

(a) JCPDS 41-1445
(b) 200-8 h
(c) 200-18 h
(d) 200-30 h
(e) 200-42 h

(C)

Figure 1: The XRD patterns of the synthesized SnO_2 nanostructures of reactions after different times and temperatures.

SnO_2 nanostructures by hydrothermal method and have studied the influence of heating time and temperature on nanostructures. This method utilizes the template of surfactant. The surfactant not only provides favorable site for the growth of the particulate assemblies, it also influences the formation process, including nucleation, growth, coagulation, and flocculation [24]. Moreover, the electrical and catalytic properties of SnO_2, especially for sensor and catalyst, have been widely studied and reported. However, the luminescence properties of SnO_2 have rarely been devoted [25]. In this paper, the room temperature photoluminescence properties of SnO_2 nanostructures are presented too. More extended investigations of this work is to establish the influences of the changing experimental parameters on the microstructural and optical characteristics of the SnO_2 nanostructures.

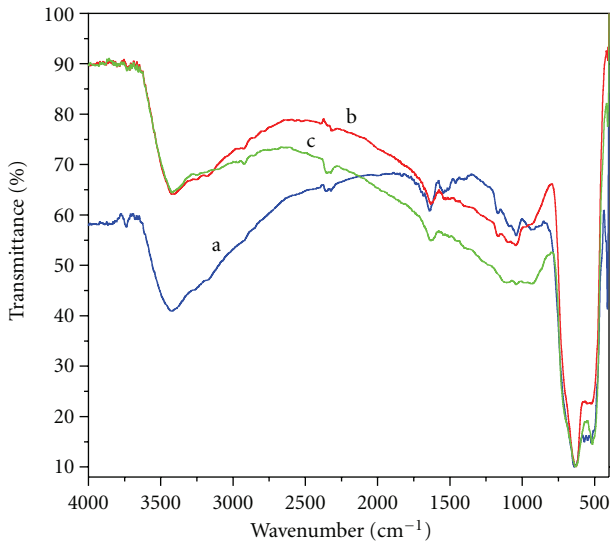

(a) 160-72 h
(b) 180-18 h
(c) 200-8 h

FIGURE 2: FT-IR spectra of the synthesized SnO_2 nanostructures of reactions after different temperatures and times: (a) 160-72 h, (b) 180-18h, and (c) 200-8 h.

2. Experimental

All the chemical reagents used in the experiments were obtained from commercial sources as guaranteed-grade reagents and used without further purification.

SnO_2 nanostructures were synthesized via a simple hydrothermal method [21]. Typically, 1.5 mL $SnCl_4 \cdot 5H_2O$ (0.52 M) was added into 4.5 mL NaOH (5.0 M) solution. After stirring 20 min, the clear solution was obtained. 4.3268 g sodium dodecyl sulphate (SDS) was dissolved in a solution consisting 9.0 mL hexanol and 30.6 mL heptane. Then, the clear solution was added into the above solution. after 20 min ultrasonic dispersing, the mixture was transferred into a 80 mL stainless Teflon-lined autoclave and maintained at 160°C, 180°C, and 200°C for different times, respectively, and afterwards allowed them to become cool in a room temperature naturally. The white precipitations at the bottom of the autoclave were collected by centrifugation, washed several times with distilled water and absolute ethanol, and finally dried at 60°C for 12 h.

Powder X-ray diffraction (XRD) data were carried out with a Rigaku D/MAX-3B powder diffractometer with copper target and K_α radiation ($\lambda = 1.54056$ Å) was used for the phase identification, where the diffracted X-ray intensities were recorded as a function of 2θ. The sample was scanned from 25° to 90° (2θ) in steps of 0.02°. Fourier transformed infrared (FTIR) spectra, in the range of 4000–400 cm^{-1}, were recorded on Perkin-Elmer 2000 FTIR spectrometer. Scanning electron microscopy (SEM) characterization was performed with FEI QUANTA200 microscope operating at 15 kV. Transmission electron microscopy (TEM) measurement was performed on a Zeiss EM 912 Ω instrument at an acceleration voltage of 120 kV, while high-resolution transmission electron microscopy (HRTEM) characterization was done using JEOL JEM-2010 Electron Microscope (with an acceleration voltage of 200 kV). The samples for TEM were prepared by dispersing the final samples in distilled deionized water; this dispersing was then dropped on carbon-copper grids covered by an amorphous carbon film. To prevent agglomeration of nanostructures the copper grid was placed on a filter paper at the bottom of a Petri dish. The Raman spectra were recorded with a Renishaw inVia Raman microscope, equipped with a CCD (charge coupled device) with the detector cooled to about 153 K using liquid N_2. The laser power was set at 300 mW. The spectral resolution was 1 cm^{-1}. UV/Vis measurements were made with a UV-2401PC spectrophotometer. Photoluminescence (PL) measurements were carried out at room temperature using 275 nm wavelength as the excitation wavelength with a Hitachi F-4500 FL Spectrophotometer with a Xe lamp as the excitation source.

3. Results and Discussion

X-ray diffraction patterns of nanostructured SnO_2 under the different hydrothermal treating temperature and time are presented in Figure 1. The present peaks in the spectra confirm the polycrystalline nature of the nanostructures, which were identified to originate of tetragonal rutile SnO_2 crystal structure with lattice constants of $a = 0.4738$ nm and $c = 0.3187$ nm. For the samples treated at 160°C for 72 h (Figure 1(A)(d)), 180°C (Figure 1(B)), or 200°C (Figure 1(C)), X-ray diffraction analysis shows that all the products are the mono-phasic with good crystallinity. The peak positions are matched well the standard data for SnO_2: JCPDS card no. 41-1445 ($a = 0.4738$ nm and $c = 0.3187$ nm). No other crystalline byproducts are found in the pattern, indicating that the as-prepared samples have a pure rutile structure. Figure 1 also shows an increase of crystallinity in the samples by the increase in the intensity of SnO_2 diffraction peaks when the hydrothermal treating temperature and time are increased. From Figure 1(A)(b) and (c), it can be seen that there are some peaks in the spectra unidentified to tetragonal rutile SnO_2, which revel the indications of other phases or crystalline byproducts in the samples. This finding implies that the hydrothermal treating temperature and time are very important to obtain the pure phasic SnO_2 with good crystallinity. A difference between the experimental and JCPDS card is observed for (101) diffraction peak. The relative intensities of (101) peak is the largest. It is a general phenomenon in the growth of the nanostructures along their direction of growth. However, the obvious preferential texturing cannot be found from the comparison between the experimental data and JCPDS card (41-1445). As can be seen from Figure 1, the diffraction peaks of SnO_2 treated at 160°C obviously broadened, which indicates the smaller particle size compared with of SnO_2 treated at 180°C and 200°C.

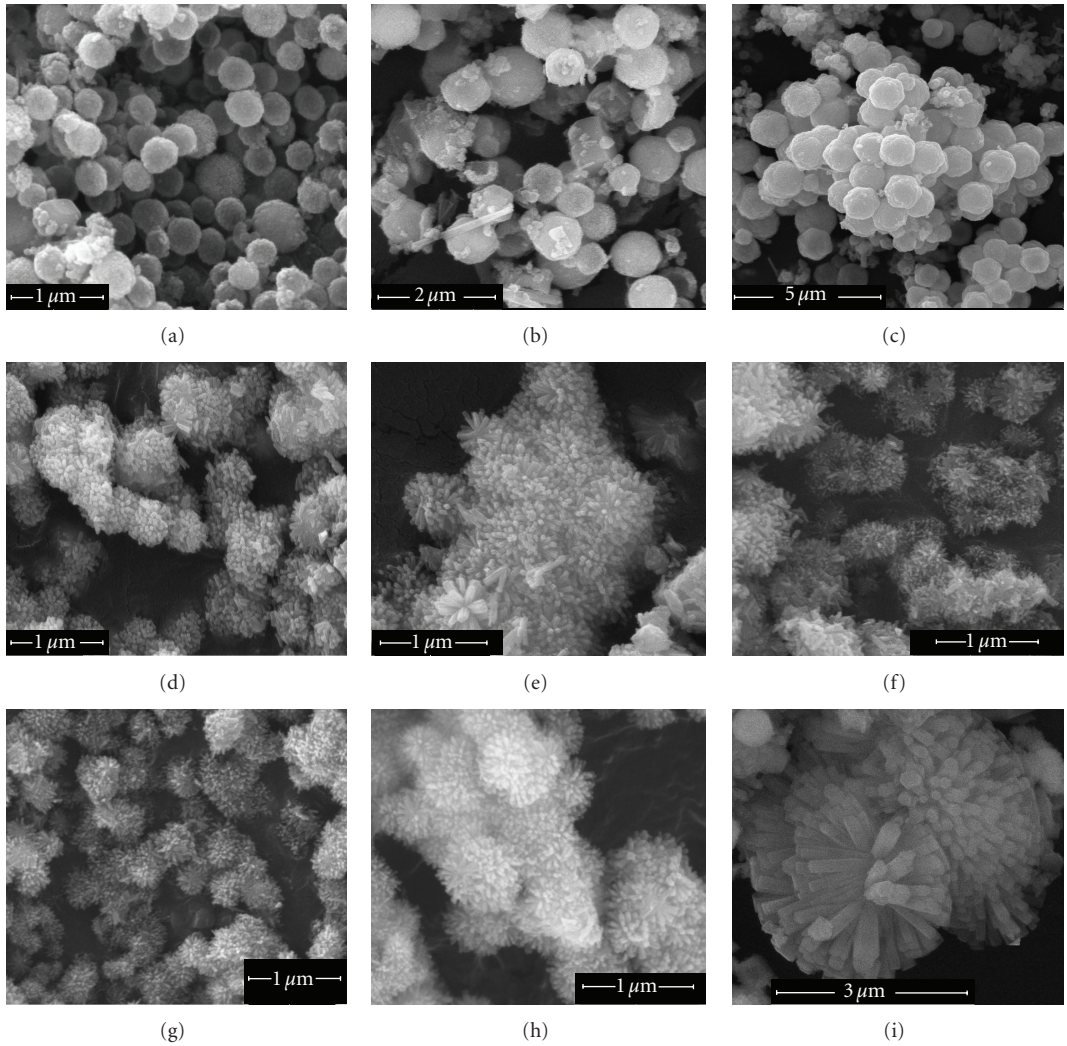

Figure 3: FE-SEM images of the synthesized SnO_2 nanostructures of reactions after different temperatures and times: (a) 160-18 h, (b) 160-42 h, (c) 160-72 h, (d) 180-18 h, (e) 180-42 h, (f) 200-8 h, (g) 200-30 h, (h) 200-42 h at low magnification, and (i) 200-42 h at high magnification.

Fourier transform infrared spectroscopy (FT-IR) was usually employed as an additional probe to evidence the presence of OH groups as well as other organic and inorganic species. For SDS, the FTIR spectrum of shows five intense bands, assigned to alkyl CH stretching (2959, 2919, and 2852 cm^{-1}) and alkyl CH deforming (1471 and 1221 cm^{-1}) [26]. The FTIR spectra in the range 4000–400 cm^{-1} of as-synthesized samples are shown in Figure 2. For the as-synthesized SnO_2 nanostructures, the inexistence of alkyl CH stretching at 2959, 2919 and 2852 cm^{-1} and alkyl CH deforming at 1471 and 1221 cm^{-1} indicates that the surfactant SDS is not present in the as-synthesized samples. The intense and broad bands at 3433 cm^{-1} and 1638 cm^{-1} can be attributed to the O–H vibration in absorbed water on the sample surface [24]. It is suggested that the high surface area of these nanostructured materials results in rapid adsorption of water from the atmosphere because the FTIR samples were kept and ground in air. The broad bands between 450 and 790 cm^{-1} are attributed to the framework vibrations of the Sn–O bond in SnO_2 [27]. The peak appeared at 634 cm^{-1} relates to the O–Sn–O bridge functional groups of SnO_2, which confirms the presence of SnO_2 as crystalline phase. This is in agreement with the results of the XRD analysis. The peak appearing at 519 cm^{-1} is due to the terminal oxygen vibration of Sn–OH.

The morphologies of the SnO_2 nanostructures were characterized by scanning electron microscopy (SEM). Figure 3 shows the detailed morphologies of the SnO_2 hollow spheres and nanorods with bush-like aggregates with hemispherical ends projecting out. The diameter of SnO_2 hollow spheres changes from 200 to 900 nm with increasing reaction time under 160°C, while the SnO_2 nanorods have a uniform length of about 100–300 nm and diameters of about 30 nm. With increasing reaction time, the aspect ratios of SnO_2 nanorods increase. Scanning electron microscope analysis for the samples synthesized under hydrothermal conditions

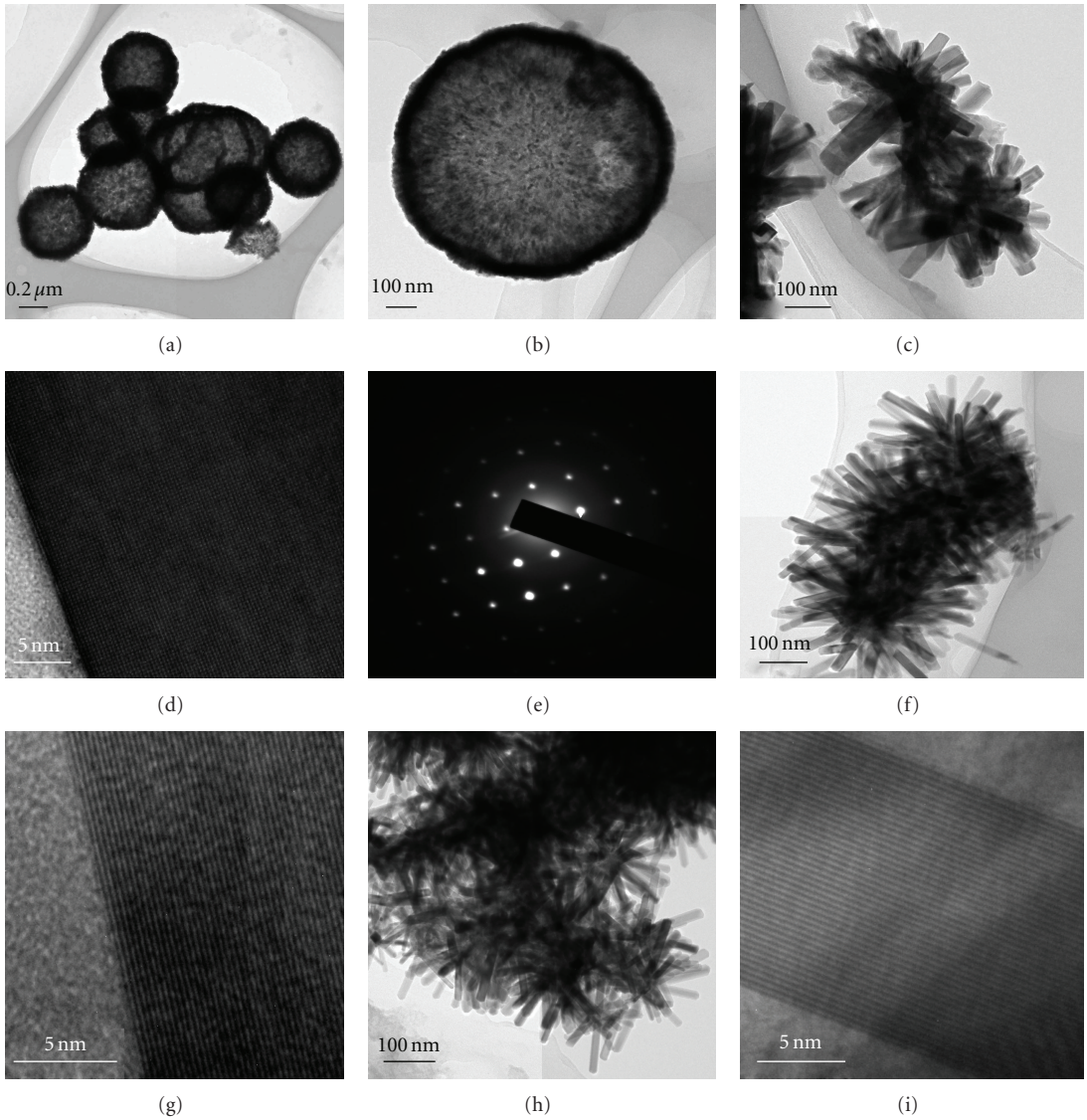

Figure 4: (a, b) TEM images of SnO_2 hollow spheres for 160-42 h sample, (c) TEM image of SnO_2 nanorods, (d) HRTEM image of a single SnO_2 nanorod, (e) SAED pattern from the individual nanorod for 180-18 h sample, (f, g) TEM image of SnO_2 nanorods and HRTEM image of a single SnO_2 nanorod for 200-8 h sample, and (h, i) TEM image of SnO_2 nanorods and HRTEM image of a single SnO_2 nanorod for 200-42 h sample.

show the influence of the hydrothermal temperature on the nanostructured morphologies. The morphology of SnO_2 was found to dependent on the synthesis conditions, which the hydrothermal temperature is the key factor, but the reaction time is not very important to morphology. As shown in Figure 3, the hollow spheres were obtained at 160°C for 18 h, 42 h and 72 h, respectively. However, the SnO_2 nanorods were obtained when the hydrothermal temperature was increased to 180 or 200°C.

TEM and high-resolution TEM (HRTEM) investigations give further insight into the morphologies and the structural features of SnO_2 hollow spheres and nanorods. The obvious contrast between the dark edge and the pale center of the spheres confirms SnO_2 hollow nature from Figures 4(a) and 4(b) for 160-42 h sample. It indicates that SnO_2 hollow spheres can be obtained under the present experimental conditions. The SnO_2 hollow spheres are in the range of 400–800 nm in diameter and in the range of 60–70 nm in shell thickness. One can see its hollow structure and clear grain boundary on the surface. It suggests that the as-obtained microspheres are constituted by aggregation of small SnO_2 particles, which is in good agreement with the XRD patterns. Figures 4(c), 4(f), and 4(h) are the typical TEM images of the as-synthesized nanorods for 180-18 h, 200-8 h and 200-42 h samples, respectively. It is clearly shows that nanorods grow homocentrically, and form urchin-like nanostructures. Their diameter and length are around 25 nm and 100–300 nm, respectively. High-resolution transmission electron microscopy (HRTEM) reveals the fine structure of the nanorods. The clear lattice fringes in the HRTEM images

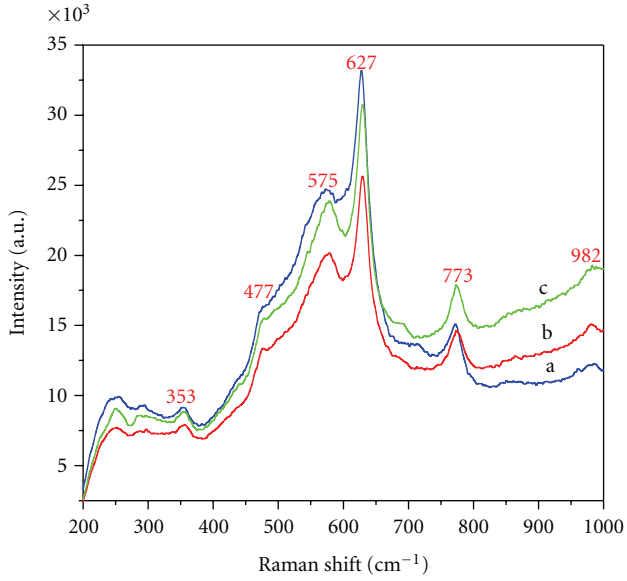

(a) 160-72 h
(b) 180-18 h
(c) 200-8 h

FIGURE 5: Room-temperature Raman spectra of the synthesized SnO_2 nanostructures.

(Figures 4(d), 4(g), and 4(i)) show the single crystal nature of the SnO_2 nanorods. The space between two adjacent lattice planes is 0.333 nm, corresponding to (110) planes of rutile SnO_2. Figure 4(e) of 180-18 h sample shows the corresponding selected area electron diffraction (SAED) pattern of the individual nanorod, indicating that the as-synthesized nanorods are single crystalline in structure. The SnO_2 nanorods of 200-8 h and 200-42 h samples show the same SAED patterns with the single crystalline in structure.

Raman scattering is a useful tool for the characterization of nanosized materials and a qualitative probe of the presence of lattice defects in solids. The formation of a tetragonal rutile structure of SnO_2 nanostructures was further supported by Raman spectra. Figure 5 presents the typical room temperature Raman spectra of the SnO_2 nanostructures for the 200–1000 cm^{-1} region. SnO_2 are tetragonal, space group $P4_2/mnm$. There are six Raman shift peaks from our samples, and the Raman spectrum of SnO_2 hollow spheres (Figure 5(a)) is much similar to that of nanorods (Figure 5(b) and (c)). The three fundamental scattering peaks at 477, 627, and 773 cm^{-1} are the three characteristic spectra of rutile SnO_2, which are in agreement with those of a rutile SnO_2 single crystal [28] and in agreement with data of group-theory analysis [29, 30]. The Raman peaks at 353 and 477 cm^{-1} are attributed to the $(E_u)\nu_{2(LO)}$ [31] and E_g vibrational modes of SnO_2. The peak at 627 cm^{-1} can be attributed to the A_{1g} symmetric Sn–O stretching mode in nanocrystalline SnO_2 and the peak at 773 cm^{-1} can be assigned to the B_{2g} vibrational mode. The Raman peaks at 575 and 982 cm^{-1} are not detected in the bulk rutile SnO_2. The Raman bands at 575 cm^{-1} are related to the small size effect according to Matossi force constant model [32]. These additional Raman peaks are similar to the Raman spectra of SnO_2 nanorods [32, 33] and nanocones [34] reported previously.

In order to reveal the possible mechanism in the formation of SnO_2 hollow spheres and nanorods, a lot of detailed hydrothermal temperature and time dependent experiments were carried out. The simple chemical reaction for the precipitation of tin oxide is proposed as follows:

$$\begin{aligned} Sn^{4+} + 6OH^- &\longrightarrow Sn(OH)_6^{2-}, \\ Sn(OH)_6^{2-} &\longrightarrow SnO_2 + 2H_2O + 2OH^-. \end{aligned} \tag{1}$$

Template-based systems are frequently used to control nucleation and growth of inorganic particles. In this approach, the SDS template simply serves as a scaffold with (or around) which a different materials is generated in situ and shaped into a nanostructure with its morphology complementary to that of the template. On the basis of the series of experimental data, the overall assembly behaviors of the SnO_2 hollow spheres and nanorods could be illustrated as in Figure 6. The similar formation mechanisms were reported and the generating hollow spheres [35] and nanostructures [21] in relatively large quantities can be synthesized by templating against or micelles assembled from SDS. In this case, the formations of the SnO_2 nanostructures belong to a self-assembly process.

UV/Vis spectroscopy was used to characterize the optical adsorptions of SnO_2 hollow spheres and nanorods. It is well known that theory of optical absorption gives the relationship between the absorption coefficients α and the photon energy $h\nu$ for direct allowed transition as [36]

$$(\alpha h\nu)^2 = B\left(h\nu - E_g\right) \tag{2}$$

in which $h\nu$ is the photon energy, E_g is the apparent optical band gap, B is a constant characteristic of the semiconductor, and α is the absorption coefficient. The direct band gap is determined using this equation when the straight portion of the $(\alpha h\nu)^2$ against $h\nu$ plot is extrapolated to intersect the energy axis at $\alpha = 0$. Figure 7 shows the graphs of $(\alpha h\nu)^2$ versus photon energy $h\nu$ for SnO_2 hollow spheres and nanorods under the different hydrothermal temperature and time. The linear part of the plot has been extrapolated towards energy axis. The intercept value on the energy axis has been found to be 3.67, 3.70, 3.73, 3.83, and 3.87 eV for 160-72 h, 180-18 h, 180-42 h, 200-8 h, and 200-42 h samples, respectively. It can be found that the optical band-gap gradually increased when the hydrothermal temperature and reaction time are increased. These optical band gaps are larger than the value of 3.62 eV for bulk SnO_2 due to the quantum size effect.

To explore the possibilities of luminescent properties by SnO_2 hollow spheres and nanorods, we carried out PL measurements at room temperature. It was reported recently that the beaklike nanorods exhibit a visible (centered at 602 nm) broad dominant photoemission peak at 300 K [37]. For the single-crystalline SnO_2 nanocauliflowers, there is

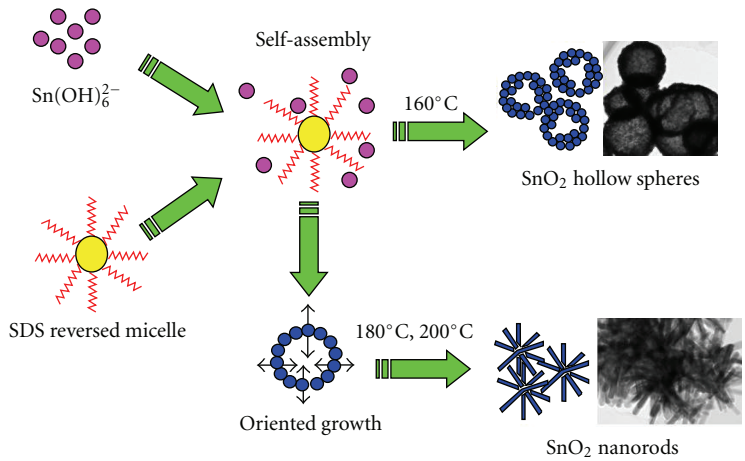

FIGURE 6: Schematic diagram of the proposed mechanism for the formation of the SnO_2 hollow spheres and nanorods at different hydrothermal temperatures.

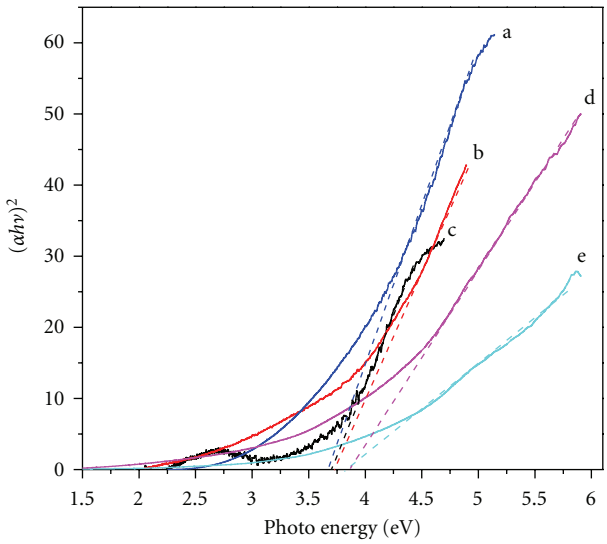

(a) 160-72 h
(b) 180-42 h
(c) 180-18 h
(d) 200-42 h
(e) 200-8 h

FIGURE 7: The optical band gap energy estimation of the SnO_2 hollow spheres and nanorods at different hydrothermal temperatures.

a strong UV emission band located at about 392 nm (3.16 eV) and a broad peak centered at about 424 nm (2.92 eV) at the room temperature [38]. Wang et al. also reported that a broad green emission band centered at 567 nm is observed in the spectrum of the SnO_2 nanorods and that centered at 535 nm is also observed in the spectrum of hollow microspheres [39]. The room temperature emission spectra of SnO_2 hollow spheres and nanorods are shown in Figure 8. In our investigation, room temperature photoluminescence spectra were performed with an excitation wavelength (λ_{ex} = 275 nm). The emission spectrum of 160-72 h sample (Figure 8(a)) gives several strong peaks at 345, 380, 398, 451, 469, 484, and 493 nm, respectively. For the samples treated at 180 and 200°C under different reaction times, the PL spectra consist of strong emission band located at 382, 398, 451, 469, 484, and 493 nm (Figure 8(b)), and 381, 398, 451, 469, 484, and 493 nm (Figure 8(c)), respectively. The emission peak at 345 nm is usually thought as origin from the free exciton electron-hole recombination [40]. The 380, 381 or 382 nm peak is attributed to the band-to-acceptor peak and related to the impurity or defect concentration and not to the structural properties [41]. The appearances of the 398 nm peak are independent of the concentration of oxygen vacancies due to structural defects or luminescent centers such as nanocrystals and defects in the SnO_2 nanostructure [41, 42]. The peaks at 469 nm are possibly attributed to electron transition mediated by defects levels in the band gap, such as oxygen vacancies [43]. However, the 451, 484, and 493 nm peaks are just found in our case. In our opinion, the three peaks may be caused by other defects or oxygen vacancies and the detailed studies on the origin of these peaks will be investigated in the future.

4. Conclusion

SnO_2 hollow spheres and nanorods were successfully prepared by an aqueous sol-gel hydrothermal route under the different hydrothermal treating temperature and time. The samples were analyzed by XRD, FTIR, SEM, TEM, and Raman spectroscopy. The characterization reveals that the samples have a tetragonal rutile structure and the hollow spheres or nanorods morphologies. The results showed that SnO_2 hollow spheres with diameters of approximately 200–900 nm and shell thickness of 60–70 nm via hydrothermal treating at 160°C and one-dimensional rod-like nanostructures with diameters of approximately 20–40 nm and lengths of 100–300 nm via hydrothermal treating at 180°C and 200°C were obtained, respectively. The effects of hydrothermal treating temperature and reaction time on the morphology characteristics and optical properties of the SnO_2 nanostructures were studied. The analysis shows that the hydrothermal treating temperature and time play a crucial

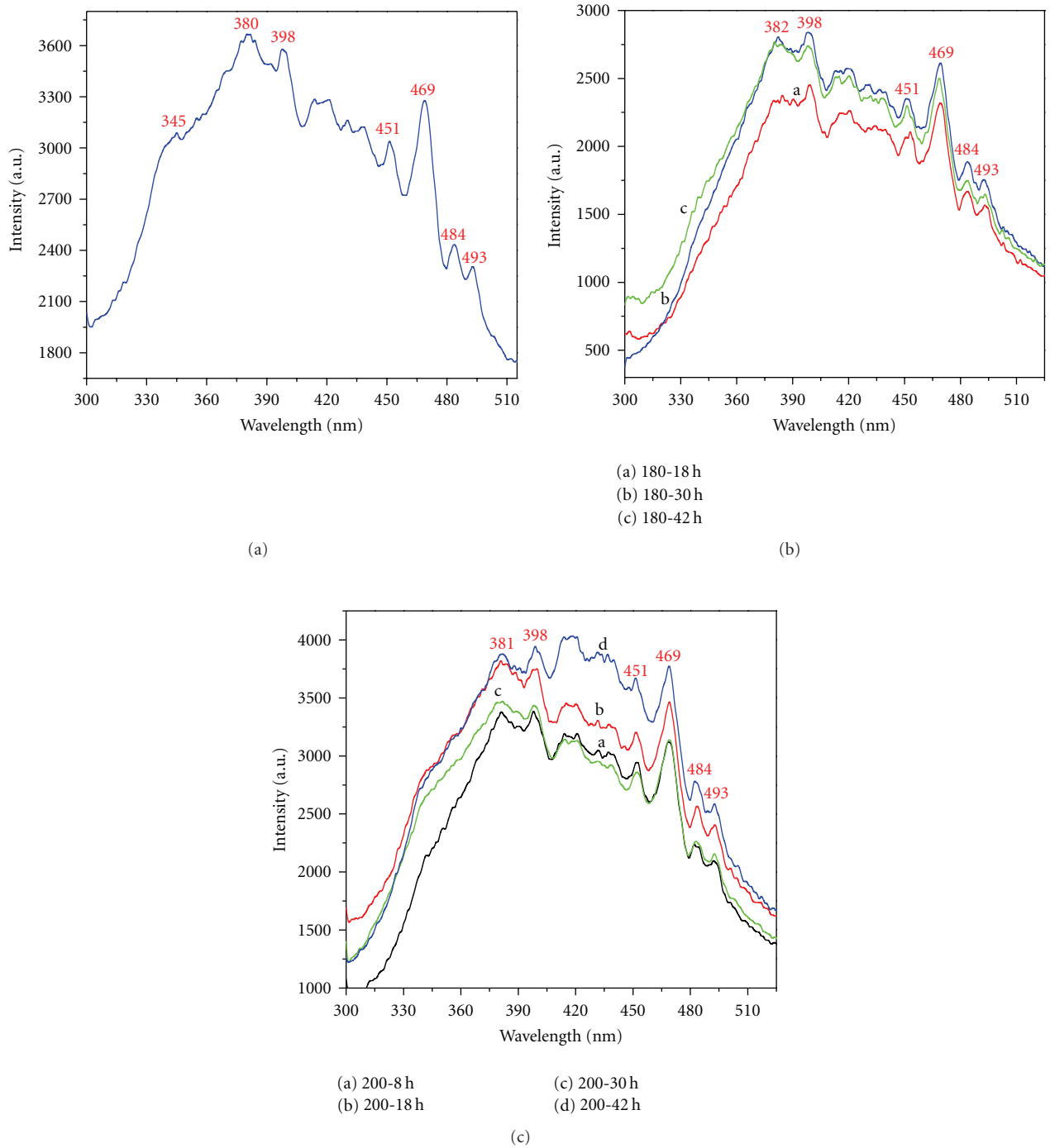

FIGURE 8: Emission (λ_{ex} = 275 nm) spectra of the synthesized SnO_2 nanostructures of reactions after different hydrothermal temperatures and times.

role to obtain the pure phasic SnO_2 with good crystallinity and the different morphology nanostructures. The optical band gaps of SnO_2 hollow spheres and nanorods are blue shifted compared with the bulk SnO_2's band gap due to the quantum size effect. PL spectra were investigated at room temperature. The 451, 484, and 493 nm emission peaks are just found for SnO_2 hollow spheres and nanorods in our case.

Acknowledgment

This work was supported by the Department of Science and Technology of Yunnan Province via the Project for the Promotion of Science and Technology (Grant no. 2009CI130) and the Key Project of Chinese Ministry of Education (no. 210206).

References

[1] C. Nayral, T. Ould-Ely, A. Maisonnat et al., "A novel mechanism for the synthesis of tin / tin oxide nanoparticles of low size dispersion of nanostructured SnO_2 for the sensitive layers of gas sensors," *Advanced Materials*, vol. 11, no. 1, pp. 61–63, 1999.

[2] E. R. Leite, I. T. Weber, E. Longo, and J. A. Varela, "A new method to control particle size and particle size distribution of SnO_2 nanoparticles for gas sensor applications," *Advanced Materials*, vol. 12, no. 13, pp. 965–968, 2000.

[3] F. L. Chen and M. L. Liu, "Preparation of mesoporous tin oxide for electrochemical applications," *Chemical Communications*, no. 18, pp. 1829–1830, 1999.

[4] Y. Fukai, Y. Kondo, S. Mori, and E. Suzuki, "Highly efficient dye-sensitized SnO_2 solar cells having sufficient electron diffusion length," *Electrochemistry Communications*, vol. 9, no. 7, pp. 1439–1443, 2007.

[5] G. A. Ozin, "Nanochemistry: synthesis in diminishing dimensions," *Advanced Materials*, vol. 4, no. 10, pp. 612–649, 1992.

[6] Y. D. Wang, C. L. Ma, X. D. Sun, and H. D. Li, "Preparation and characterization of SnO_2 nanoparticles with a surfactant-mediated method," *Nanotechnology*, vol. 13, no. 5, pp. 565–569, 2002.

[7] J. Q. Hu, X. L. Ma, N. G. Shang et al., "Large-scale rapid oxidation synthesis of SnO_2 nanoribbons," *Journal of Physical Chemistry B*, vol. 106, no. 15, pp. 3823–3826, 2002.

[8] Y. Liu, J. Dong, and M. Liu, "Well-aligned 'nano-box-beams' of SnO_2," *Advanced Materials*, vol. 16, no. 4, pp. 353–356, 2004.

[9] J. H. Ba, J. Polleux, M. Antonietti, and M. Niederberger, "Non-aqueous synthesis of tin oxide nanocrystals and their assembly into ordered porous mesostructures," *Advanced Materials*, vol. 17, no. 20, pp. 2509–2512, 2005.

[10] S. J. Han, B. C. Jang, T. Kim, S. M. Oh, and T. H. Hyeon, "Simple synthesis of hollow tin dioxide microspheres and their application to lithium-ion battery anodes," *Advanced Functional Materials*, vol. 15, no. 11, pp. 1845–1850, 2005.

[11] E. R. Leite, I. T. Weber, E. Longo, and J. A. Varela, "A new method to control particle size and particle size distribution of SnO_2 nanoparticles for gas sensor applications," *Advanced Materials*, vol. 12, no. 13, pp. 965–968, 2000.

[12] G. S. Pang, S. G. Chen, Y. Koltypin, A. Zaban, S. Feng, and A. Gedanken, "Controlling the particles size of calcined SnO_2 nanocrystals," *Nano Letters*, vol. 1, no. 12, pp. 723–726, 2001.

[13] T. C. Yeh, K. M. Hickman, S. C. Goel, A. M. Viano, P. C. Gibbons, and W. E. Buhro, "Solution-liquid-solid growth of crystalline III-V semiconductors: an analogy to vapor-liquid-solid growth," *Science*, vol. 270, no. 5243, pp. 1791–1794, 1995.

[14] Z. Q. Liu, D. H. Zhang, S. Han et al., "Laser ablation synthesis and electron transport studies of tin oxide nanowires," *Advanced Materials*, vol. 15, no. 20, pp. 1754–1757, 2003.

[15] Y. L. Wang, X. C. Jiang, and Y. N. Xia, "A solution-phase, precursor route to polycrystalline SnO_2 nanowires that can be used for gas sensing under ambient conditions," *Journal of the American Chemical Society*, vol. 125, no. 52, pp. 16176–16177, 2003.

[16] Q. R. Zhao, Y. Gao, X. Bai, C. Wu, and Y. Xie, "Facile synthesis of SnO_2 hollow nanospheres and applications in gas sensors and electrocatalysts," *European Journal of Inorganic Chemistry*, vol. 2006, no. 8, pp. 1643–1648, 2006.

[17] H. Wang, J. Liang, H. Fan et al., "Synthesis and gas sensitivities of SnO_2 nanorods and hollow microspheres," *Journal of Solid State Chemistry*, vol. 181, no. 1, pp. 122–129, 2008.

[18] L. Vayssieres and M. Graetzel, "Highly ordered SnO_2 nanorod arrays from controlled aqueous growth," *Angewandte Chemie International Edition*, vol. 43, no. 28, pp. 3666–3670, 2004.

[19] Z. J. Miao, Y. Y. Wu, X. R. Zhang et al., "Large-scale production of self-assembled SnO_2 nanospheres and their application in highperformance chemiluminescence sensors for hydrogen sulfide gas," *Journal of Materials Chemistry*, vol. 17, no. 18, pp. 1791–1796, 2007.

[20] X. W. Lou, Y. Wang, C. Yuan, J. Y. Lee, and L. A. Archer, "Template-free synthesis of SnO_2 hollow nanostructures with high lithium storage capacity," *Advanced Materials*, vol. 18, no. 17, pp. 2325–2329, 2006.

[21] D. F. Zhang, L. D. Sun, J. L. Yin, and C. H. Yan, "Low-temperature fabrication of highly crystalline SnO_2 nanorods," *Advanced Materials*, vol. 15, no. 12, pp. 1022–1025, 2003.

[22] M. Krishna and S. Komarneni, "Conventional- vs microwave-hydrothermal synthesis of tin oxide, SnO_2 nanoparticles," *Ceramics International*, vol. 35, no. 8, pp. 3375–3379, 2009.

[23] M. N. A. Karlsson, K. Deppert, L. S. Karlsson, M. H. Magnusson, J. O. Malm, and N. S. Srinivasan, "Compaction of agglomerates of aerosol nanoparticles: a compilation of experimental data," *Journal of Nanoparticle Research*, vol. 7, no. 1, pp. 43–49, 2005.

[24] G. L. Zou, R. Liu, W. X. Chen, and Z. D. Xu, "Preparation and characterization of lamellar-like $Mg(OH)_2$ nanostructures via natural oxidation of Mg metal in formamide/water mixture," *Materials Research Bulletin*, vol. 42, no. 6, pp. 1153–1158, 2007.

[25] S. K. Pillai, L. M. Sikhwivhilu, and T. K. Hillie, "Synthesis, characterization and photoluminescence properties of Dy^{3+}-doped nano-crystalline SnO_2," *Materials Chemistry and Physics*, vol. 120, no. 2-3, pp. 619–624, 2010.

[26] N. Gungor, A. Alemdar, O. Atici, and I. O. Ece, "The effect of SDS surfactant on the flow and zeta potential of bentonite suspensions," *Materials Letters*, vol. 51, no. 3, pp. 250–254, 2001.

[27] J. Zhang and L. Gao, "Synthesis and characterization of nanocrystalline tin oxide by sol-gel method," *Journal of Solid State Chemistry*, vol. 177, no. 4-5, pp. 1425–1430, 2004.

[28] J. F. Scott, "Raman spectrum of SnO_2," *The Journal of Chemical Physics*, vol. 53, no. 2, pp. 852–853, 1970.

[29] H. Kohno, T. Iwasaki, Y. Mita, and S. Takeda, "One-phonon Raman scattering studies of chains of crystalline-Si nanospheres," *Journal of Applied Physics*, vol. 91, no. 5, pp. 3232–3235, 2002.

[30] V. G. Kravets, "Photoluminescence and Raman spectra of SnO_x nanostructures doped with Sm ions," *Optics and Spectroscopy*, vol. 103, no. 5, pp. 766–771, 2007.

[31] O. Lupan, L. Chow, G. Chai, A. Schulte, S. Park, and H. Heinrich, "A rapid hydrothermal synthesis of rutile SnO_2 nanowires," *Materials Science and Engineering B*, vol. 157, no. 1–3, pp. 101–104, 2009.

[32] Y. J. Chen, L. Nie, X. Y. Xue, Y. G. Wang, and T. H. Wang, "Linear ethanol sensing of SnO_2 nanorods with extremely high sensitivity," *Applied Physics Letters*, vol. 88, no. 8, Article ID 083105, 2006.

[33] B. Cheng, J. M. Russell, W. Shi, L. Zhang, and E. T. Samulski, "Large-scale, solution-phase growth of single-crystalline SnO_2 nanorods," *Journal of the American Chemical Society*, vol. 126, no. 19, pp. 5972–5973, 2004.

[34] G. Cheng, J. Wang, X. Liu, and K. Huang, "Self-assembly synthesis of single-crystalline tin oxide nanostructures by a poly(acrylic acid)-assisted solvothermal process," *Journal of Physical Chemistry B*, vol. 110, no. 33, pp. 16208–16211, 2006.

[35] Q. Zhao, Y. Gao, X. Bai, C. Wu, and Y. Xie, "Facile synthesis of SnO_2 hollow nanospheres and applications in gas sensors and electrocatalysts," *European Journal of Inorganic Chemistry*, no. 8, pp. 1643–1648, 2006.

[36] G. Mills, Z. G. Li, and D. Meisel, "Photochemistry and spectroscopy of colloidal arsenic sesquisulfide," *Journal of Physical Chemistry*, vol. 92, no. 3, pp. 822–828, 1988.

[37] J. H. He, T. H. Wu, C. L. Hsin et al., "Beaklike SnO_2 nanorods with strong photoluminescent and field-emission properties," *Small*, vol. 2, no. 1, pp. 116–120, 2006.

[38] Y. Wang, M. Guo, M. Zhang, and X. Wang, "Template-free hydrothermal synthesis of single-crystalline SnO_2 nanocauliflowers and their optical properties," *Rare Metals*, vol. 28, no. 5, pp. 449–453, 2009.

[39] H. Z. Wang, J. B. Liang, H. Fan et al., "Synthesis and gas sensitivities of SnO_2 nanorods and hollow microspheres," *Journal of Solid State Chemistry*, vol. 181, no. 1, pp. 122–129, 2008.

[40] E. J. H. Lee, C. Ribeiro, T. R. Giraldi, E. Longo, E. R. Leite, and J. A. Varela, "Photoluminescence in quantum-confined SnO_2 nanocrystals: evidence of free exciton decay," *Applied Physics Letters*, vol. 84, no. 10, pp. 1745–1747, 2004.

[41] J. Jeong, S. P. Choi, C. I. Chang et al., "Photoluminescence properties of SnO_2 thin films grown by thermal CVD," *Solid State Communications*, vol. 127, no. 9-10, pp. 595–597, 2003.

[42] T. W. Kim, D. U. Lee, and Y. S. Yoon, "Microstructural, electrical, and optical properties of SnO_2 nanocrystalline thin films grown on InP (100) substrates for applications as gas sensor devices," *Journal of Applied Physics*, vol. 88, no. 6, pp. 3759–3761, 2000.

[43] F. Gu, S. F. Wang, M. K. Lü, G. J. Zhou, D. Xu, and D. R. Yuan, "Photoluminescence properties of SnO_2 nanoparticles synthesized by sol-gel method," *Journal of Physical Chemistry B*, vol. 108, no. 24, pp. 8119–8123, 2004.